J. Fluid Mech. (2007), *vol.* 581, *pp.* 401–418.
doi:10.1017/S0022112007005873 Printed in the United Kingdom

Local stability analysis of an inviscid transverse jet

LEONARDO S. DE B. ALVES, ROBERT E. KELLY AND ANN R. KARAGOZIAN

Department of Mechanical and Aerospace Engineering, University of California, Los Angeles, Los Angeles, CA 90095-1597, USA

(Received 18 August 2006 and in revised form 4 January 2007)

A local linear stability analysis is performed for a round inviscid jet with constant density that is injected into a uniform crossflow of the same density. The baseflow is obtained from a modified version of the inviscid transverse jet near-field solution of Coelho & Hunt (*J. Fluid Mech.* vol. 200, 1989, p. 95) which is valid for small values of the crossflow-to-jet velocity ratio λ. A Fourier expansion in the azimuthal direction is used to couple the disturbances with the three-dimensional crossflow. The spatial growth rates of the modes corresponding to the axisymmetric and first helical modes of the free jet as $\lambda \to 0$ increase as λ increases. The diagonal dominance of the dispersion relation matrix is used as a quantitative criterion to estimate the range of velocity ratios ($0 < \lambda < \lambda_c$) within which the transverse jet instability can be considered to have a structure similar to that of the free jet. Further, we show that for $\lambda > 0$ positive and negative helical modes have different growth rates, suggesting an inherent weak asymmetry in the transverse jet.

1. Introduction

The jet in crossflow (or transverse jet) is a flow field that appears in a variety of technological applications such as in propulsion systems, where transverse air jets are used for temperature pattern factor control and/or emission control, for fuel injection, and for thrust vector control. A more detailed description of the variety of possible applications of the transverse jet can be found in Margason (1993) and Karagozian, Cortelezzi & Soldati (2003).

The jet injected normally from a wall into a crossflow involves two fundamental flows: a perpendicular free jet and a boundary-layer driven by uniform flow far above the injection wall. The transverse jet's characteristics are far more complex than those present in these basic canonical flows, however. As the jet exits the nozzle or pipe, which can be either flush-mounted in the wall or protruding into the crossflow, it is deflected by the crossflow until both flows become aligned in the same direction. A schematic of this complicated interaction process for flush injection is shown in figure 1, where a variety of coherent structures are formed: (i) the jet's shear-layer vortices; (ii) wake vortices downstream of the jet; (iii) a counter-rotating vortex pair (CVP) generally associated with the jet's cross-section, and (iv) horse-shoe vortices forming about the jet orifice.

In the present work, we are interested in the first of these structures, which form for both flush and elevated jet injection (Megerian *et al.* 2006) and are widely thought to be generated by the well-known Kelvin–Helmholtz inviscid instability mechanism (Kelso, Lim & Perry 1996; Fric & Roshko 1994). Yet some researchers argue that the

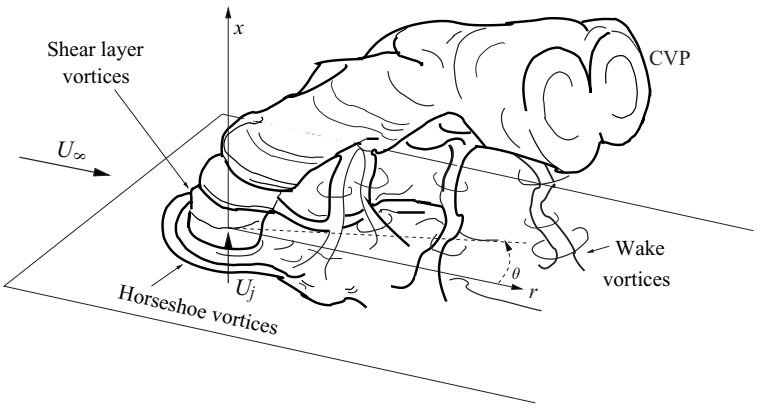

FIGURE 1. Schematic of the jet in crossflow and associated vortical structures, after Fric & Roshko (1994). Coordinate system for the present analysis is shown.

transverse jet shear layer instability is strongly influenced by the near-field formation and longitudinal evolution of the CVP and hence is not precisely of the Kelvin–Helmholtz type (Huq & Dhanak 1996; Blanchard, Brunet & Merlen 1999). To explore this and other issues, linear stability analysis is carried out in the present study using the inviscid vortex-sheet solution of Coelho & Hunt (1989) as a baseflow, which contains discontinuities in the velocity profile. This solution has been extended by Coelho (1988) and Needham, Riley & Smith (1988) to represent inclined jets in crossflow. It is well known that the use of discontinuous velocity profiles to represent open shear layer flows, such as in the planar mixing layer or the free jet, yields linear disturbances with spatial (or temporal) growth rates that increase monotonically with frequency (or wavenumber). Although such a result is not realistic, since a maximum growth rate does exist for continuous velocity profiles, it does agree well with experimental and numerical results obtained from continuous velocity profiles in the limit of small frequencies (or wavenumbers) (see Chandrasekhar 1961; Drazin & Reid 1981; Godrèche & Manneville 1998; Lin 2003 for details), and useful trends and phenomena may be extracted. The present study involving a local linear stability analysis (LSA) of an inviscid baseflow is one of several transverse jet studies currently being pursued by our group; these include the LSA of a continuous base flow (Alves, Kelly & Karagozian 2006), full numerical simulations (Alves 2006), and experimental exploration (Megerian *et al.* 2006).

Shear layer instabilities in free jets are more complex than in their planar mixing layer counterparts due to the existence of a second characteristic length scale in addition to the jet momentum thickness, that is, the jet diameter. As a direct consequence, disturbances with different azimuthal modes may be present in the flow field at different streamwise locations. The work of Batchelor & Gill (1962) was among the first to explore instability of a free jet. They use two different models for the free jet: a top-hat profile and a continuous solution. Although Batchelor & Gill perform a temporal linear stability analysis, Crow & Champagne (1971) extend the analysis to include spatial instability. These latter authors are also among the first to have studied and controlled the evolution of large-scale coherent structures in a turbulent free jet, achieving maximum amplification of the disturbances present at the nozzle exit through forcing of specific frequencies, consistent with the concept of a convectively unstable flow (Huerre & Monkewitz 1990). Hence in the present study we consider the flow field of the jet to be locally convectively unstable and the

transverse jet disturbances to evolve spatially, because the same is true for the free jet and because the crossflow-to-jet velocity ratio λ is assumed to be small.

To our knowledge, there is no work in the available literature that has used linear stability techniques to investigate the effect of a crossflow on jet shear layer instabilities. Blossey & Schmid (2002) report some preliminary results on a large-scale global stability analysis that used time-averaged direct numerical simulation (DNS) data as a baseflow. It is found that the growth rates of the shear layer modes increase and that these modes appear closer to the jet exit as the jet Reynolds number is increased, but the results were obtained for only a single value of λ ($= 1/6$). We pursue a different approach here, using a simple and computationally inexpensive baseflow model in order to obtain information concerning the instability of the transverse jet for a wide range of λ.

The transverse jet inviscid baseflow model used in the present study is based on the one developed by Coelho & Hunt (1989). An error exists in one of the second-order kinematic conditions derived by Coelho (1988), and while this does not affect the results in Coelho & Hunt (1989), it is important in the present analysis. In the present paper, we correct this problem in § 2 and describe the new inviscid three-dimensional solution for the steady transverse jet. Then, we show in § 3 how a Fourier expansion is used to analyse the stability problem and to obtain a dispersion relation. Finally, we present in § 4 the spatial growth rates of the inviscid transverse jet using this linear stability approach. Asymmetry of the flow is also discussed there.

2. Baseflow

The inviscid incompressible three-dimensional vortex-sheet model of Coelho & Hunt (1989) for the near field of a strong jet issuing from a pipe into a uniform crossflow is the foundation for our analysis. Asymptotic solutions are represented in integral powers of the small parameter $\lambda \equiv U_\infty/U_j$, the crossflow-to-jet velocity ratio. The lowest-order solution is a circular jet with uniform velocity that is bounded by a vortex sheet. The boundary-value problem is formulated in cylindrical coordinates (x, r and θ) where θ is measured with respect to the downstream or lee side of the jet, as shown in figure 1. The problem is shown by Coelho & Hunt to yield the following results for the velocity potentials ϕ_j and ϕ_e for the internal and external regions of the jet, respectively:

$$\phi_j = \phi_j^{(0)} + \lambda\phi_j^{(1)} + \lambda^2\phi_j^{(2)} + O(\lambda^3) = x + \lambda^2 F_2(x,r)\cos[2\theta] + O(\lambda^3), \quad r \leqslant R_j, \tag{2.1a}$$

$$\phi_e = \phi_e^{(0)} + \lambda\phi_e^{(1)} + \lambda^2\phi_e^{(2)} + O(\lambda^3) = \lambda\left(r + \frac{1}{r}\right)\cos[\theta] + O(\lambda^3), \quad r > R_j, \tag{2.1b}$$

where the function $F_2(x,r)$ is given by

$$F_2(x,r) = (C_2 - x)r^2 + \sum_{n=1}^{\infty} A_n J_2[\sigma_n r]\exp[-\sigma_n x], \quad x \geqslant 0, \tag{2.1c}$$

$$F_2(x,r) = \sum_{n=1}^{\infty} B_n J_2[\tau_n r]\exp[+\tau_n x], \quad x \leqslant 0, \tag{2.1d}$$

with σ_n and τ_n being the zeros of the Bessel function J_2 and its derivative, respectively. The near-field evolution of the cross-sectional shape R_j of the transverse jet is

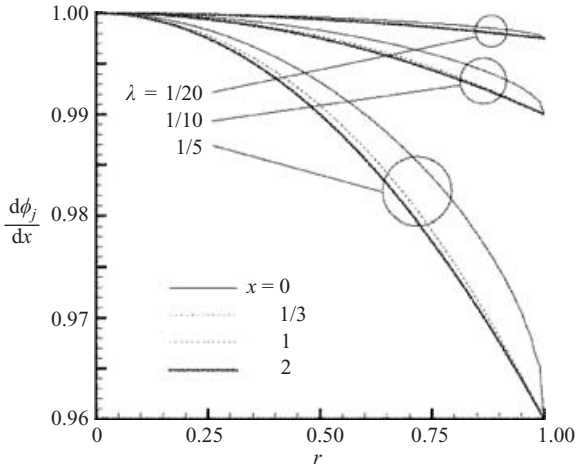

FIGURE 2. Inviscid streamwise velocity component behaviour in the radial and streamwise directions for different values of λ at $\theta = 0$.

represented by

$$R_j = 1 - \lambda^2 \left\{ x(x - 2C_2) - \sum_{n=1}^{\infty} A_n J_3[\sigma_n](\exp[-\sigma_n x] - 1) \right\} \cos[2\theta]. \tag{2.1e}$$

In the above, the variables are made dimensionless by use of the nozzle exit radius R_0 and velocity U_j. The numerical values of the coefficients C_2, A_n and B_n are determined by enforcing continuity of the velocity potential ϕ_j and its derivatives across the nozzle exit at $x = 0$, and taking advantage of the orthogonality of the Bessel functions. The linear system of equations that determines B_n is

$$\sum_{m=1}^{\infty} \frac{B_m \tau_m J_2(\tau_m)}{\sigma_m - \tau_m} = -\frac{1}{\sigma_n}, \tag{2.2a}$$

which enables us to evaluate A_n and C_2 from

$$A_n = \frac{2}{\sigma_n J_3(\sigma_n)} \sum_{m=1}^{\infty} \frac{B_m \tau_m^2 J_2(\tau_m)}{\sigma_m^2 - \tau_m^2} \quad \text{and} \quad C_2 = \sum_{m=1}^{\infty} B_m J_2(\tau_m). \tag{2.2b, c}$$

The summation terms associated with the exponential decay in x due to the exit effects present in relations (2.1c) and (2.1e) become negligible for $x > 1/3$. This is demonstrated in figure 2, which shows the streamwise velocity component variation with x, r and λ at $\theta = 0$, the lee side of the jet. The variation with x of $\partial\phi_j/\partial x$ is due entirely to these exponential terms. Because of this, we can simplify F_2 and R_j when $x > 1/3$ as

$$F_2(x, r) = (C_2 - x)r^2, \tag{2.3a}$$

$$R_j = 1 - \lambda^2 \left\{ x(x - 2C_2) + \sum_{n=1}^{\infty} A_n J_3[\sigma_n] \right\} \cos[2\theta]. \tag{2.3b}$$

At this point we note that a detailed analysis of the derivation by Coelho (1988) shows that the $O(\lambda^2)$ kinematic condition for the external flow needs to be corrected because it neglects the deformation of the interface. If one ignores the exponentially

decaying terms in x, equation (2.1b) for ϕ_e may be replaced by the corrected relation:

$$\phi_e = \lambda\left(r + \frac{1}{r}\right)\cos[\theta] - \lambda^2\left(\frac{C_2 - x}{r^2}\right)\cos[2\theta] + O(\lambda^3), \quad r > R_j. \tag{2.4}$$

All the other solutions presented above remain the same as in Coelho & Hunt (1989).

The impact this correction has on the results presented by Coelho & Hunt (1989) is minimal. Most of the models these researchers develop are compared with each other and with their own experimental data, using the transverse jet cross-sectional shape R_j, such as the one given in (2.1e). This function is only affected by equation (2.4) at the $O(\lambda^3)$ problem, but their analysis is performed only up to order λ^2. Nevertheless, this correction is important for the present work and will be retained throughout this study.

The inviscid velocity profiles at each order in λ are then obtained from

$$U_i(x, r, \theta) = \frac{\partial \phi^{(i)}}{\partial x}, \quad V_i(x, r, \theta) = \frac{\partial \phi^{(i)}}{\partial r}, \quad W_i(x, r, \theta) = \frac{1}{r}\frac{\partial \phi^{(i)}}{\partial \theta}, \quad i = 0, 1, 2, \ldots. \tag{2.5}$$

Because the flow is assumed to be inviscid, a vortex sheet exists and a discontinuity is present in the above solution at $r = 1$. The flow for $r > 1$ is the same as that past a circular cylinder to $O(\lambda)$, but the flow is fully three-dimensional everywhere at $O(\lambda^2)$.

3. Linear stability analysis

This section describes the general steps needed in order to derive the linear disturbance equations. Then, the details on the approach used to solve the linear stability problem are provided before presenting results. All the equations and results from the stability analysis in this paper are obtained using the symbolic and numerical computation capabilities of the software *Mathematica* created by Wolfram (1999).

3.1. *Governing equations and interface conditions*

The governing equations within the transverse jet, written in terms of the overall velocity potential (denoted by an asterisk), are the continuity equation

$$\nabla \cdot \boldsymbol{u} = \nabla^2 \phi_j^* = \frac{\partial^2 \phi_j^*}{\partial x^2} + \frac{1}{r}\frac{\partial}{\partial r}\left(r\frac{\partial \phi_j^*}{\partial r}\right) + \frac{1}{r^2}\frac{\partial^2 \phi_j^*}{\partial \theta^2} = 0, \tag{3.1a}$$

which is valid everywhere except at the vortex sheet, and the Bernoulli equation

$$\frac{\partial \phi_j^*}{\partial t} + \frac{1}{2}\nabla \phi_j^* \cdot \nabla \phi_j^* + \frac{P_j^*}{\rho} = \text{const}, \tag{3.1b}$$

where ρ is the density of the jet and of the crossflow.

Outside the transverse jet, the continuity equation becomes

$$\nabla \cdot \boldsymbol{u} = \nabla^2 \phi_e^* = \frac{\partial^2 \phi_e^*}{\partial x^2} + \frac{1}{r}\frac{\partial}{\partial r}\left(r\frac{\partial \phi_e^*}{\partial r}\right) + \frac{1}{r^2}\frac{\partial^2 \phi_e^*}{\partial \theta^2} = 0, \tag{3.2a}$$

whereas the Bernoulli equation becomes

$$\frac{\partial \phi_e^*}{\partial t} + \frac{1}{2}\nabla \phi_e^* \cdot \nabla \phi_e^* + \frac{P_e^*}{\rho} = \text{const}. \tag{3.2b}$$

On the interface $\mathscr{S} = r - r^*(x, \theta, t) = 0$, the kinematic conditions are

$$\frac{\partial \mathscr{S}}{\partial t} + \nabla \phi_j^* \cdot \nabla \mathscr{S} = 0 \quad \text{and} \quad \frac{\partial \mathscr{S}}{\partial t} + \nabla \phi_e^* \cdot \nabla \mathscr{S} = 0, \tag{3.3a, b}$$

and the dynamic condition $P_j^* = P_e^*$ allows us to write

$$\frac{\partial \phi_j^*}{\partial t} + \frac{1}{2}\nabla\phi_j^* \cdot \nabla\phi_j^* = \frac{\partial \phi_e^*}{\partial t} + \frac{1}{2}\nabla\phi_e^* \cdot \nabla\phi_e^*. \tag{3.3c}$$

3.2. *Linearization and normal mode analysis*

Coelho & Hunt's modified solution (mean quantities ϕ_j, ϕ_e and R_j) is now perturbed by introducing infinitesimal disturbances not only for the velocity potential (disturbance quantities $\widetilde{\phi}_j$ and $\widetilde{\phi}_e$) but for the interface displacement as well (disturbance quantity $\widetilde{R}_j$). Because the free jet is sensitive to local disturbances that render the flow convectively unstable (see Huerre & Monkewitz 1990), we expect the same to be true for the transverse jet, at least for small values of λ, which is consistent with recent experimental observations by Megerian *et al.* (2006). We therefore assume that these disturbances evolve spatially and can be separated into Fourier modes as follows:

$$\phi_j^* = \phi_j + \widetilde{\phi}_j = \phi_j + \Phi_j(r,\theta)\exp[\mathrm{i}(\alpha x - \omega t)], \tag{3.4a}$$

$$\phi_e^* = \phi_e + \widetilde{\phi}_e = \phi_e + \Phi_e(r,\theta)\exp[\mathrm{i}(\alpha x - \omega t)], \tag{3.4b}$$

$$R_j^* = R_j + \widetilde{R}_j = R_j + \mathscr{N}(\theta)\exp[\mathrm{i}(\alpha x - \omega t)], \tag{3.4c}$$

with $\mathrm{i} \equiv \sqrt{-1}$, and ϕ_j, ϕ_e and R_j given by relations (2.1*a*), (2.4) and (2.3*b*). Since we assume that disturbances grow spatially, the wavenumber α is taken to be a complex number and the frequency ω is an arbitrary real number. A local stability analysis is performed in this study, which is the reason why the x dependence of Φ_j, Φ_e and $\mathscr{N}$ is ignored in (3.4). From this point on, $x = x_0$ becomes a parameter for these terms in our analysis at $O(\lambda^2)$.

Substituting relations (3.4) into equations (3.1*a*) and (3.2*a*) we obtain

$$\frac{1}{r}\frac{\partial}{\partial r}\left(r\frac{\partial \Phi_j}{\partial r}\right) + \frac{1}{r^2}\frac{\partial^2 \Phi_j}{\partial \theta^2} - \alpha^2 \Phi_j = 0, \tag{3.5a}$$

which is valid inside the transverse jet, and

$$\frac{1}{r}\frac{\partial}{\partial r}\left(r\frac{\partial \Phi_e}{\partial r}\right) + \frac{1}{r^2}\frac{\partial^2 \Phi_e}{\partial \theta^2} - \alpha^2 \Phi_e = 0, \tag{3.5b}$$

which is valid outside the transverse jet.

Based on (3.4*c*), we can approximate on a linear basis the value of an arbitrary function f at the disturbed interface by the relation

$$f(x, R_j^*, \theta, t) \simeq f(x, R_j, \theta, t) + \widetilde{R}_j \left.\frac{\partial f}{\partial r}\right|_{r=R_j} + \cdots. \tag{3.6}$$

Making use of (3.4), we write the kinematic conditions (3.3*a*, *b*), respectively, as

$$\left\{-\mathrm{i}\left(\omega - \alpha\frac{\partial \phi_j}{\partial x}\right)\mathscr{N} + \frac{1}{r}\frac{\partial \phi_j}{\partial \theta}\frac{1}{r}\frac{\mathrm{d}\mathscr{N}}{\mathrm{d}\theta} = \frac{\partial \Phi_j}{\partial r} - \mathrm{i}\alpha\Phi_j\frac{\partial R_j}{\partial x} - \frac{1}{r}\frac{\partial \Phi_j}{\partial \theta}\frac{1}{r}\frac{\partial R_j}{\partial \theta}\right\}_{r=R_j}, \tag{3.7a}$$

$$\left\{-\mathrm{i}\left(\omega - \alpha\frac{\partial \phi_e}{\partial x}\right)\mathscr{N} + \frac{1}{r}\frac{\partial \phi_e}{\partial \theta}\frac{1}{r}\frac{\mathrm{d}\mathscr{N}}{\mathrm{d}\theta} = \frac{\partial \Phi_e}{\partial r} - \mathrm{i}\alpha\Phi_e\frac{\partial R_j}{\partial x} - \frac{1}{r}\frac{\partial \Phi_e}{\partial \theta}\frac{1}{r}\frac{\partial R_j}{\partial \theta}\right\}_{r=R_j}. \tag{3.7b}$$

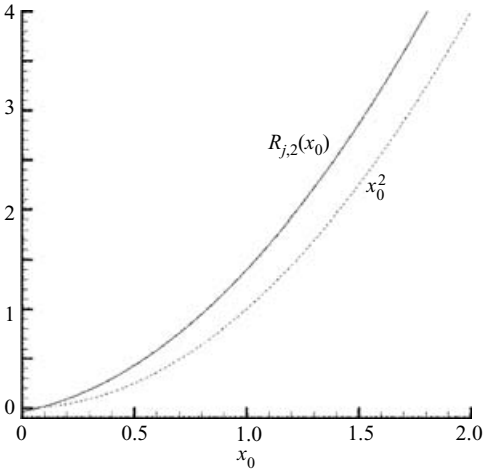

FIGURE 3. Second-order correction to interface position $R_{j,2}(x_0)$ as a function of downstream location x_0, with $R_{j,2}(0) \simeq -0.036368$.

Similarly, we can write the dynamic condition (3.3*c*) as

$$\left\{-\mathrm{i}\left(\omega-\alpha\frac{\partial\phi_j}{\partial x}\right)\Phi_j+\frac{\partial\phi_j}{\partial r}\frac{\partial\Phi_j}{\partial r}+\frac{1}{r}\frac{\partial\phi_j}{\partial\theta}\frac{1}{r}\frac{\partial\Phi_j}{\partial\theta}\right.$$
$$\left.=-\mathrm{i}\left(\omega-\alpha\frac{\partial\phi_e}{\partial x}\right)\Phi_e+\frac{\partial\phi_e}{\partial r}\frac{\partial\Phi_e}{\partial r}+\frac{1}{r}\frac{\partial\phi_e}{\partial\theta}\frac{1}{r}\frac{\partial\Phi_e}{\partial\theta}\right\}_{r=R_j}. \quad (3.7c)$$

A further approximation is also introduced. The kinematic and dynamic conditions (3.7) must be evaluated at the transverse jet interface R_j, which depends on λ as shown in equation (2.3*b*). Hence, we use a Taylor series expansion to approximate the value of any baseflow quantity at the deformed interface as

$$f(R_j,\theta;x_0)\simeq f(1,\theta;x_0)+\lambda^2R_{j,2}(x_0)\cos[2\theta]\left.\frac{\partial f}{\partial r}\right|_{r=1}+\cdots, \quad (3.8)$$

where $R_{j,2}(x_0)$ represents the term within braces in equation (2.3*b*). The behaviour of $R_{j,2}(x_0)$ is shown in figure 3 for reference and compared to x_0^2. This suggests that we need $(x_0\lambda)^2 \ll 1$ for the expansion to be valid, along with $\lambda \ll 1$.

3.3. *Multiple mode approach*

In order to take into account the coupling, due to the baseflow, between different azimuthal modes in our analysis, we will solve the governing equations (3.5) and (3.7) considering multiple modes simultaneously through the use of Fourier expansions. A perturbation expansion in terms of λ is presented in Alves (2006) but the Fourier expansion is thought to have a wider range of applicability. Approximation (3.8) is first applied to the kinematic and dynamic conditions (3.7). Here, we take advantage of the fact that our baseflow is accurate up to $O(\lambda^2)$ and neglect higher-order terms in λ present in the approximate interface conditions. Neglecting $R_j'(x)$ as well, on the basis that it represents a non-local effect, and substituting the baseflow (2.1*a*) and

(2.4), the approximate kinematic and dynamic conditions become

$$(1+2\lambda^2\cos[2\theta]R_{j,2}(x_0))\left.\frac{\partial\Phi_j}{\partial r}\right|_{r=1}+\lambda^2\cos[2\theta]R_{j,2}(x_0)\left.\frac{\partial^2\Phi_j}{\partial r^2}\right|_{r=1}$$
$$=-\mathrm{i}(\omega-\alpha)\mathscr{N}(\theta)-\lambda^2\Bigg(\mathrm{i}\cos[2\theta](\alpha+2(\omega-\alpha)R_{j,2}(x_0))\mathscr{N}(\theta)$$
$$+2\sin[2\theta]\left((C_2-x_0)\frac{\mathrm{d}\mathscr{N}}{\mathrm{d}\theta}+R_{j,2}(x_0)\left.\frac{\partial\Phi}{\partial\theta}\right|_{r=1}\right)\Bigg), \tag{3.9a}$$

$$(1+2\lambda^2\cos[2\theta]R_{j,2}(x_0))\left.\frac{\partial\Phi_e}{\partial r}\right|_{r=1}+\lambda^2\cos[2\theta]R_{j,2}(x_0)\left.\frac{\partial^2\Phi_e}{\partial r^2}\right|_{r=1}$$
$$=-\mathrm{i}\omega\mathscr{N}(\theta)-2\lambda\sin[\theta]\frac{\mathrm{d}\mathscr{N}}{\mathrm{d}\theta}+\lambda^2\Bigg(\mathrm{i}\cos[2\theta](\alpha-2\omega R_{j,2}(x_0))\mathscr{N}(\theta)$$
$$+2\sin[2\theta]\left((C_2-x_0)\frac{\mathrm{d}\mathscr{N}}{\mathrm{d}\theta}-R_{j,2}(x_0)\left.\frac{\partial\Phi}{\partial\theta}\right|_{r=1}\right)\Bigg), \tag{3.9b}$$

$$-\mathrm{i}((\omega-\alpha)+\lambda^2(\alpha+2(\omega-\alpha)R_{j,2}(x_0))\cos[2\theta])\Phi_j(1,\theta)$$
$$-2\lambda^2(C_2-x_0)\sin[2\theta]\left.\frac{\partial\Phi_j}{\partial\theta}\right|_{r=1}+\lambda^2(2(C_2-x_0)-\mathrm{i}(\omega-\alpha)R_{j,2}(x_0))\cos[2\theta]\left.\frac{\partial\Phi_j}{\partial r}\right|_{r=1}$$
$$=-i(\omega+\lambda^2(2\omega R_{j,2}(x_0)-\alpha)\cos[2\theta])\Phi_e(1,\theta)-2\lambda(\sin[\theta]$$
$$-\lambda(C_2-x_0)\sin[2\theta])\left.\frac{\partial\Phi_e}{\partial\theta}\right|_{r=1}+\lambda^2(2(C_2-x_0)-\mathrm{i}\omega R_{j,2}(x_0))\cos[2\theta]\left.\frac{\partial\Phi_e}{\partial r}\right|_{r=1}. \tag{3.9c}$$

Now we use the Fourier transformation pairs

$$\Phi_j(r,\theta)=\sum_{m=-\infty}^{\infty}\overline{\Phi}_{j,m}(r)\exp[\mathrm{i}m\theta]\quad\text{and}\quad\overline{\Phi}_{j,m}(r)=\frac{1}{2\pi}\int_0^{2\pi}\Phi_j(r,\theta)\exp[-\mathrm{i}m\theta]\,\mathrm{d}\theta, \tag{3.10a}$$

$$\Phi_e(r,\theta)=\sum_{m=-\infty}^{\infty}\overline{\Phi}_{e,m}(r)\exp[\mathrm{i}m\theta]\quad\text{and}\quad\overline{\Phi}_{e,m}(r)=\frac{1}{2\pi}\int_0^{2\pi}\Phi_e(r,\theta)\exp[-\mathrm{i}m\theta]\,\mathrm{d}\theta, \tag{3.10b}$$

$$\mathscr{N}(\theta)=\sum_{m=-\infty}^{\infty}\overline{\mathscr{N}}_m\exp[\mathrm{i}m\theta]\quad\text{and}\quad\overline{\mathscr{N}}_m=\frac{1}{2\pi}\int_0^{2\pi}\mathscr{N}(\theta)\exp[-\mathrm{i}m\theta]\,\mathrm{d}\theta. \tag{3.10c}$$

Multiplying the interface conditions (3.9*a–c*) by $\exp[-\mathrm{i}m\theta]/2\pi$, integrating the result from 0 to 2π and substituting the inversion formulae in (3.10) where necessary, we obtain the Fourier-transformed interface conditions

$$2\pi(\overline{\Phi}'_{j,m}(1)+\mathrm{i}(\omega-\alpha)\overline{\mathscr{N}}_m)+\lambda^2\sum_{n=-\infty}^{\infty}\Big[\big(2(C_2-x_0)\mathscr{M}^{(3)}_{m,n}$$
$$+\mathrm{i}(\alpha+2(\omega-\alpha)R_{j,2}(x_0))\mathscr{M}^{(1)}_{m,n}\big)\overline{\mathscr{N}}_n+2R_{j,2}(x_0)\mathscr{M}^{(3)}_{m,n}\overline{\Phi}_{j,n}(1)$$
$$+R_{j,2}(x_0)\mathscr{M}^{(1)}_{m,n}(2\overline{\Phi}'_{j,n}(1)+\overline{\Phi}''_{j,n}(1))\Big]=0, \tag{3.11a}$$

$$2\pi(\overline{\Phi}'_{j,m}(1)+\mathrm{i}\omega\overline{\mathscr{N}}_m)+\lambda\sum_{n=-\infty}^{\infty}\Big[\big(2\mathscr{M}^{(2)}_{m,n}$$
$$+\lambda\big(\mathrm{i}\mathscr{M}^{(1)}_{m,n}(2\omega R_{j,2}(x_0)-\alpha)-2(C_2-x_0)\mathscr{M}^{(3)}_{m,n}\big)\big)\overline{\mathscr{N}}_n$$
$$+\lambda R_{j,2}(x_0)\big(2\mathscr{M}^{(3)}_{m,n}\overline{\Phi}_{e,n}(1)+\mathscr{M}^{(1)}_{m,n}(2\overline{\Phi}'_{e,n}(1)+\overline{\Phi}''_{e,n}(1))\big)\Big]=0, \tag{3.11b}$$

$$2\pi\mathrm{i}(\omega-\alpha)\overline{\Phi}_{j,m}(1)+\lambda^2\sum_{n=-\infty}^{\infty}\big[\big(2(C_2-x_0)\mathscr{M}^{(3)}_{m,n}+\mathrm{i}\mathscr{M}^{(1)}_{m,n}(\alpha+2R_{j,2}(x_0)(\omega-\alpha))\big)\overline{\Phi}_{j,n}(1)-\mathscr{M}^{(1)}_{m,n}\big(2(C_2-x_0)-\mathrm{i}R_{j,2}(x_0)(\omega-\alpha)\big)\overline{\Phi}'_{j,n}(1)\big]=2\pi\mathrm{i}\omega\overline{\Phi}_{e,m}(1)+\lambda\sum_{n=-\infty}^{\infty}\big[\big(2\mathscr{M}^{(2)}_{m,n}-\lambda\big(\mathrm{i}(\alpha-2\omega R_{j,2}(x_0))\mathscr{M}^{(1)}_{m,n}+2(C_2-x_0)\mathscr{M}^{(3)}_{m,n}\big)\big)\overline{\Phi}_{e,n}(1)+\lambda(\mathrm{i}\omega R_{j,2}(x_0)-2(C_2-x_0))\mathscr{M}^{(1)}_{m,n}\overline{\Phi}'_{e,n}(1)\big], \tag{3.11c}$$

where the integral matrix coefficients $\mathscr{M}^{(1)}_{m,n}$, $\mathscr{M}^{(2)}_{m,n}$ and $\mathscr{M}^{(3)}_{m,n}$ are defined as

$$\mathscr{M}^{(1)}_{m,n}=\int_0^{2\pi}\cos[2\theta]\exp[\mathrm{i}(n-m)\theta]\mathrm{d}\theta\rightarrow\begin{pmatrix}0&0&\pi&0&0\\0&0&0&\pi&0\\\pi&0&0&0&\pi\\0&\pi&0&0&0\\0&0&\pi&0&0\end{pmatrix}, \tag{3.12a}$$

$$\mathscr{M}^{(2)}_{m,n}=\mathrm{i}n\int_0^{2\pi}\sin[\theta]\exp[\mathrm{i}(n-m)\theta]\mathrm{d}\theta\rightarrow\begin{pmatrix}0&\pi&0&0&0\\-2\pi&0&0&0&0\\0&-\pi&0&\pi&0\\0&0&0&0&-2\pi\\0&0&0&\pi&0\end{pmatrix}, \tag{3.12b}$$

$$\mathscr{M}^{(3)}_{m,n}=\mathrm{i}n\int_0^{2\pi}\sin[2\theta]\exp[\mathrm{i}(n-m)\theta]\mathrm{d}\theta\rightarrow\begin{pmatrix}0&0&0&0&0\\0&0&0&-\pi&0\\-2\pi&0&0&0&-2\pi\\0&-\pi&0&0&0\\0&0&0&0&0\end{pmatrix}, \tag{3.12c}$$

and evaluated from $m,n=-2$ to 2 in order to show the structure of these matrix coefficients and demonstrate the coupling they introduce.

Before proceeding any further, we Fourier transform the disturbance continuity equations (3.5*a*, *b*) using definitions (3.10*a*) to obtain

$$\frac{1}{r}\frac{\mathrm{d}}{\mathrm{d}r}\left(r\frac{\mathrm{d}\overline{\Phi}_{j,m}}{\mathrm{d}r}\right)-\left(\alpha^2+\frac{m^2}{r^2}\right)\overline{\Phi}_{j,m}=0, \tag{3.13a}$$

$$\frac{1}{r}\frac{\mathrm{d}}{\mathrm{d}r}\left(r\frac{\mathrm{d}\overline{\Phi}_{e,m}}{\mathrm{d}r}\right)-\left(\alpha^2+\frac{m^2}{r^2}\right)\overline{\Phi}_{e,m}=0, \tag{3.13b}$$

which have the following boundary conditions:

$$\overline{\Phi}_{j,m}(r\rightarrow 0)=\text{finite}\quad\text{and}\quad\overline{\Phi}_{e,m}(r\rightarrow\infty)=0. \tag{3.13c}$$

The solution to these equations are given in terms of the modified Bessel functions

$$\overline{\Phi}_{j,m}=\mathscr{G}_{1,m}I_m(\alpha r)\quad\text{and}\quad\overline{\Phi}_{e,m}=\mathscr{G}_{2,m}K_m(\alpha r), \tag{3.14a, b}$$

where $\mathscr{G}_{1,m}$ and $\mathscr{G}_{2,m}$ are, together with $\overline{\mathscr{N}}_m$, constants to be determined.

Substituting solutions (3.14) into the kinematic and dynamic interface conditions (3.11) and truncating the resulting system of equations so as to analyse a finite number

N_m of azimuthal modes, we obtain the matrix whose determinant is the transverse jet's dispersion relation

$$D^{(N_m)} = D^{(N_m)}(\alpha; \omega, x_0, \lambda) = 0. \tag{3.15}$$

It is noted that no assumptions have been made so far about the transverse jet symmetry in this analysis of multiple modes.

4. Results and discussion

Now we present and discuss the results obtained from the linear stability analysis of the inviscid transverse jet presented in § 3.3. The multiple mode analysis allows us to investigate the effect of the coupling between different azimuthal modes and the inherent asymmetry of the transverse jet, as discussed separately in the following subsections.

4.1. *Mode coupling*

According to a separate perturbation analysis (Alves 2006), the solvability conditions for $\pm m$ azimuthal modes are equivalent. This implies that the transverse jet could have a plane of symmetry similar to the one found for the free jet. For now we impose this symmetry condition in the current multiple mode analysis by setting

$$\mathscr{G}_{1,m} = \mathscr{G}_{1,-m}, \quad \mathscr{G}_{2,m} = \mathscr{G}_{2,-m}. \quad \overline{\mathscr{N}}_m = \overline{\mathscr{N}}_{-m}. \tag{4.1}$$

The original free jet dispersion relation is recovered from the transverse jet dispersion relation as $\lambda \to 0$. In this limit, the dispersion matrix is diagonal and the azimuthal modes are decoupled. The crossflow introduces a mode coupling into the hydrodynamic stability of the flow, however, that becomes stronger as the crossflow-to-jet velocity ratio λ increases. A direct consequence of this is that, as λ increases, more and more modes will need to be introduced in the analysis in order to converge the results associated with the first azimuthal modes in the Fourier expansion. This can be observed in table 1, which shows the behaviour of the wavenumber and growth rate of the axisymmetric, first and second helical modes as the total number of modes used in the analysis increases. By the term 'axisymmetric' here we mean that the growth rate approaches the value for the axisymmetric mode of the free jet as $\lambda \to 0$; similar interpretations hold also for the other modes. The non-dimensional frequency can be identified as a Strouhal number, St. When $St = 1.90986$ and $\lambda = 0.1$, a 3 digit convergence (maximum absolute error $\simeq 0.018$) of the axisymmetric mode's complex wavenumber is obtained using a total of 13 modes ($N_m = 12$) in the calculations. However, such convergence is only achieved for the first and second helical modes with a total of 29 modes ($N_m = 28$).

The fact that the coupling between different azimuthal modes becomes significant for a value of λ even as small as 0.1 leads us to an open question in the literature regarding the similarities between free and transverse jets: What is the range of velocity ratios ($0 < \lambda < \lambda_c$) within which the transverse jet still behaves as a free jet? As mentioned previously, the free jet dispersion relation is diagonal, but the transverse jet dispersion relation is not. From the perspective of the jet's shear layer instability, therefore, the present analysis can be used to establish a simple quantitative criterion to help determine λ_c. In the present study, λ_c represents the maximum value of λ for which the transverse jet dispersion relation matrix is still diagonally dominant, i.e. as long as $\lambda < \lambda_c$, the non-diagonal terms that introduce the coupling are small enough so that the free and transverse jets can be assumed similar. While strict diagonal

N_m	$\alpha_{m=0}$	$\alpha_{m=1}$	$\alpha_{m=2}$
1	5.74855 − 5.74065i	5.82837 − 5.82643i	*N/A*
2	5.76676 − 5.87397i	5.88340 − 5.86821i	5.68823 − 5.54465i
3	5.88618 − 5.89345i	5.77948 − 5.94233i	5.74246 − 5.76588i
4	5.79168 − 5.88193i	5.88631 − 5.89796i	5.77521 − 6.03926i
5	5.87472 − 5.90345i	5.83704 − 5.95025i	5.80432 − 5.78218i
6	5.82028 − 5.88269i	5.85724 − 6.04146i	5.86995 − 5.92084i
7	5.86448 − 5.89681i	5.87377 − 5.96117i	5.84244 − 5.80586i
8	5.83562 − 5.88847i	5.88977 − 6.05563i	5.89876 − 5.89945i
9	5.85971 − 5.88673i	5.89547 − 5.97387i	5.87044 − 5.82993i
10	5.84306 − 5.89060i	5.90722 − 6.06247i	5.90966 − 5.90740i
11	5.85245 − 5.88247i	5.91156 − 5.98514i	5.89564 − 5.84846i
12	5.84693 − 5.89033i	5.92221 − 6.06859i	5.89327 − 5.76413i
13	5.84862 − 5.88380i	5.92413 − 5.99589i	5.91324 − 5.86057i
14	5.84879 − 5.88922i	5.93427 − 6.07535i	5.90654 − 5.78469i
15	5.84747 − 5.88537i	5.93433 − 6.00604i	5.92536 − 5.87135i
16	5.84944 − 5.88806i	5.94413 − 6.08205i	5.91768 − 5.80244i
17	5.84736 − 5.88644i	5.94293 − 6.01573i	5.93459 − 5.88173i
18	5.84940 − 5.88721i	5.95260 − 6.08854i	5.92733 − 5.81799i
19	5.84763 − 5.88706i	5.95034 − 6.02511i	5.94214 − 5.89189i
20	5.84908 − 5.88674i	5.96015 − 6.09487i	5.93577 − 5.83186i
21	5.84798 − 5.88733i	5.95681 − 6.03429i	5.94864 − 5.90195i
22	5.84872 − 5.88658i	5.96710 − 6.10107i	5.94317 − 5.84448i
23	5.84829 − 5.88737i	5.96249 − 6.04329i	5.95444 − 5.91199i
24	5.84844 − 5.88662i	5.96241 − 5.98104i	5.94966 − 5.85624i
25	5.84850 − 5.88727i	5.96757 − 6.05213i	5.94629 − 5.79448i
26	5.84830 − 5.88675i	5.96810 − 5.99115i	5.95543 − 5.86673i
27	5.84839 − 5.88715i	5.97539 − 6.06015i	5.96569 − 5.91264i
28	5.84842 − 5.88728i	5.96471 − 6.04474i	5.95844 − 5.91519i

TABLE 1. Complex wavenumber convergence in multiple mode analysis for $St = 1.90986$, $x_0 = 1$ and $\lambda = 0.1$.

dominance cannot be imposed because the dispersion relation matrix is singular, we can establish this criterion mathematically by defining the following equation for λ_c:

$$\left|D_{i,i}^{(N_m)}(\lambda_c)\right| = \sum_{j=1(j\neq i)}^{N_m} \left|D_{i,j}^{(N_m)}(\lambda_c)\right| \quad \text{for any } i \neq m, \tag{4.2}$$

with m being the azimuthal number of the chosen disturbance. In the equation above, the left-hand side represents the diagonal terms whereas the right-hand side represents the non-diagonal terms. As long as LHS > RHS, the matrix is diagonally dominant. When the opposite is true, diagonal dominance is lost and the transverse jet shear layer instability becomes fundamentally different from that for the round free jet. Hence, equation (4.2) yields the value of λ at which the matrix transitions from one case to the other, i.e. it yields a necessary condition for λ_c. The first mode to lose its diagonal dominance is the axisymmetric mode, with $\lambda_c \simeq 0.0036$. The first and second helical modes lose their diagonal dominance when $\lambda_c \simeq 0.0063$ and $\lambda_c \simeq 0.0069$, respectively. We note that criterion (4.2) is very conservative since it is applied independently to each line i in the dispersion relation matrix. Further, the values of λ_c are calculated using $N_m = 6$, 7 and 8 in order to verify the convergence of results. While few experimental studies (or applications) exist for transverse jets with such a low crossflow-to-jet velocity ratio, these findings demonstrate that the

λ	$\alpha_{m=0}$	$\alpha_{m=1}$	$\alpha_{m=2}$
		$St = 0.63662$	
0	1.66274 − 1.75551i	1.86795 − 1.64688i	2.01936 − 1.75211i
0.01	1.66274 − 1.75551i	1.86895 − 1.64705i	2.02007 − 1.74896i
0.02	1.66274 − 1.75551i	1.87202 − 1.64753i	2.02277 − 1.73812i
0.05	1.66277 − 1.75555i	1.89645 − 1.65117i	2.00933 − 1.50091i
0.1	1.66396 − 1.75666i	1.97807 − 1.69701i	1.63185 − 1.04803i
		$St = 0.95493$	
0	2.75252 − 2.74371i	2.75974 − 2.69699i	2.89434 − 2.67008i
0.01	2.75250 − 2.74371i	2.76140 − 2.69818i	2.89659 − 2.66839i
0.02	2.75211 − 2.74377i	2.76669 − 2.70173i	2.90367 − 2.66364i
0.05	2.74587 − 2.75333i	2.80782 − 2.71778i	2.94984 − 2.64201i
0.1	2.75054 − 2.80541i	2.93215 − 2.76901i	2.98459 − 2.46888i
		$St = 1.27324$	
0	3.74750 − 3.73481i	3.76012 − 3.72534i	3.81228 − 3.68681i
0.01	3.74740 − 3.73498i	3.76284 − 3.72803i	3.81545 − 3.68612i
0.02	3.74724 − 3.73698i	3.77058 − 3.73442i	3.82473 − 3.68468i
0.05	3.75627 − 3.75894i	3.80963 − 3.76595i	3.87969 − 3.68507i
0.1	3.80253 − 3.84327i	3.91953 − 3.85444i	3.95335 − 3.59346i
		$St = 1.59155$	
0	4.74745 − 4.73903i	4.75714 − 4.73037i	4.78609 − 4.70826i
0.01	4.74728 − 4.73943i	4.76176 − 4.73457i	4.79003 − 4.70921i
0.02	4.74777 − 4.74278i	4.77362 − 4.74477i	4.80105 − 4.71215i
0.05	4.76322 − 4.76863i	4.82734 − 4.80383i	4.86391 − 4.73170i
0.1	4.83058 − 4.85952i	4.93730 − 4.96133i	4.94365 − 4.69311i
		$St = 1.90986$	
0	5.74855 − 5.74065i	5.75451 − 5.73472i	5.77416 − 5.71895i
0.01	5.74841 − 5.74156i	5.76093 − 5.74016i	5.77970 − 5.72174i
0.02	5.75027 − 5.74616i	5.77679 − 5.75379i	5.79415 − 5.72965i
0.05	5.77119 − 5.77741i	5.85598 − 5.83803i	5.86937 − 5.77042i
0.1	5.84842 − 5.88728i	5.96471 − 6.04474i	5.95844 − 5.91519i

TABLE 2. Complex wavenumber from multiple mode analysis. The maximum absolute error of the first helical mode is approximately 1.8×10^{-2} at $\lambda = 0.1$, 1.0×10^{-4} at $\lambda = 0.05$, 1.5×10^{-14} at $\lambda = 0.02$ and 3.8×10^{-25} at $\lambda = 0.01$. The second helical mode has absolute errors of the same order, which is several orders of magnitude higher than the axisymmetric mode errors.

transverse jet instabilities are fundamentally different from those in the free jet, even for very weak crossflows.

The complex wavenumber behaviour with respect to the velocity ratio of the first three azimuthal numbers is presented in table 2, where the free jet solution ($\lambda = 0$) is shown for reference. In the perturbation analysis of Alves (2006), the $O(\lambda^2)$ connection to the growth rate of the axisymmetric mode is found to be zero. An important consequence of the mode coupling is the fact that it allows the crossflow to influence the axisymmetric mode. This can be seen in table 2, which shows that the axisymmetric mode growth rate $-\mathrm{Im}[\alpha_{m=0}]$ increases with λ for all five Strouhal numbers presented. Table 2 also shows that this increase becomes more pronounced

at higher frequencies. A similar behaviour is also observed for the first helical mode, with the growth rate increase with frequency being the most pronounced among all three modes shown. The second helical mode growth rate does increase with λ at higher frequencies, but this behaviour is reversed as the frequency decreases, with the switch occurring at $St \simeq 1.3$.

The behaviour of the helical modes described by the multiple mode analysis is qualitatively similar to that predicted by the perturbation expansion analysis (Alves 2006). But the more interesting result obtained from this analysis is the destabilization of the axisymmetric mode by the crossflow, which occurs due to the coupling between different modes and the axisymmetric mode. Such destabilization of the jet's axisymmetric mode by the crossflow is consistent with observations in recent transverse jet shear layer experiments, which indicate the strengthening of convective instabilities. Such convective instabilities for the transverse jet are observed in experiments to occur closer to the jet orifice than those associated with the free jet, and as crossflow magnitude increases, the instability is strengthened in magnitude (Megerian *et al.* 2006). It is also interesting to note that in the present study the growth rates of both helical modes for the transverse jet are higher than that of the axisymmetric mode for high enough values of St (and λ), contrary to trends observed in the free jet (Crow & Champagne 1971).

4.2. *Flow asymmetry*

The present analysis may also be used to explore inherent asymmetries associated with the transverse jet. Free jets issuing from circular pipes or nozzles are often referred to as 'axisymmetric jets' due to the geometric symmetry of the experimental apparatus or numerical model (see Corke, Shakib & Nagib 1991). In such cases, when the noise level is low and random, the mean velocity profile can be considered symmetric. However, if helical disturbances for some reason exceed axisymmetric ones in amplitude at the jet inlet, the axial symmetry of the mean profile is lost (see Corke & Kusek 1993). The mean profile might still possess a plane of symmetry in such cases, but only if helical disturbance pairs $\pm m$ have the same amplitude. This understanding is corroborated by the spatial linear stability analysis of Michalke (1971), which shows that axisymmetric disturbances are more unstable than helical ones for free jets with thin shear layers and that the growth rate of helical disturbances is independent of the sign of the azimuthal mode number m. Hence the free jet is regarded axisymmetric close to the nozzle exit from the perspective of an open shear flow. This symmetry concept can be extended to transverse jets, at least for low enough crossflow-to-jet velocity ratios λ where this flow is expected to be convectively unstable, just like its free jet counterpart.

To explore the possibility of asymmetry in the multiple mode approach, the symmetry constraint (4.1) is removed and the original dispersion relation (3.15) is used. It turns out that this original dispersion relation is not independent of the sign of the azimuthal number m. In order to demonstrate this result, it is sufficient to investigate the three (or two, depending on interpretation) mode problem $m = 0$ and ± 1. Since so few modes are used, the kinematic and dynamic conditions (3.11) can be easily combined in such a way as to eliminate $\overline{\mathscr{N}}_m$ and $\mathscr{G}_{1,m}$ so that the transverse jet dispersion relation matrix reduces to

$$\boldsymbol{D}^{(3)} = \begin{pmatrix} D_{1,1} & 0 & D_{1,3} \\ D_{2,3} & D_{2,2} & D_{2,3} \\ D_{1,3} & 0 & D_{1,1} \end{pmatrix}, \tag{4.3}$$

where the expressions for the $D_{i,j}$ matrix coefficients are given in the Appendix. It is important to note that $D_{1,3} \to 0$ and $D_{2,3} \to 0$ as $\lambda \to 0$, and that the diagonal terms in matrix (4.3) are the original free jet dispersion relation terms.

The complex wavenumbers of interest are the eigenvalues of matrix (4.3), and are obtained by setting its determinant to be zero, yielding

$$\left(D_{1,1}^2 - D_{1,3}^2\right) D_{2,2} = 0, \tag{4.4a}$$

which can be split into two separate equations

$$D_{1,1}^2 - D_{1,3}^2 = 0 \quad \text{and} \quad D_{2,2} = 0. \tag{4.4b,c}$$

These equations are decoupled from each other, with (4.4*c*) yielding the complex wavenumber associated with the axisymmetric mode $m = 0$. Hence, by only considering modes $m = 0$ and ± 1 in this analysis, we find that the crossflow does not affect the original free jet axisymmetric mode. The first equation can be split into two different equations, $D_{1,1} = +D_{1,3}$ and $D_{1,1} = -D_{1,3}$, one for each mode $m = \pm 1$. Hence, the growth rates of the $m = \pm 1$ modes will be different from each other for non-zero values of λ, although both modes converge to the free jet first helical mode as $\lambda \to 0$ since $D_{1,3} \to 0$ in this limit.

In order to further validate this finding, and also to verify if this particular asymmetry affects other helical modes, we repeat the above derivation, but now include azimuthal modes $m = \pm 2$ and perform a five (or three, again depending on interpretation) mode analysis. In this case, the transverse jet dispersion relation matrix reduces to

$$\boldsymbol{D}^{(5)} = \begin{pmatrix} D_{1,1} & D_{1,2} & D_{1,3} & D_{1,4} & D_{1,5} \\ D_{2,1} & D_{2,2} & D_{2,3} & D_{2,4} & D_{2,5} \\ D_{3,1} & D_{3,2} & D_{3,3} & D_{3,2} & D_{3,1} \\ D_{2,5} & D_{2,4} & D_{2,3} & D_{2,2} & D_{2,1} \\ D_{1,5} & D_{1,4} & D_{1,3} & D_{1,2} & D_{1,1} \end{pmatrix}, \tag{4.5}$$

where the expressions for the $D_{i,j}$ matrix coefficients are not given here due to their complexity. Nevertheless, all off-diagonal terms in matrix (4.5) vanish as $\lambda \to 0$, as they did in matrix (4.3). However, contrary to matrix (4.3), the diagonal terms in matrix (4.5) do contain corrections due to the crossflow, although they vanish as $\lambda \to 0$.

The complex wavenumbers of interest are the eigenvalues of matrix (4.5) and are obtained by setting its determinant to zero. As done with (4.4*a*), the resulting equation can be split into two different equations

$$(D_{1,1} - D_{1,5})(D_{2,2} - D_{2,4}) - (D_{1,2} - D_{1,4})(D_{2,1} - D_{2,5}) = 0, \tag{4.6a}$$

$$\begin{aligned} &2D_{1,3}((D_{2,2} + D_{2,4})D_{3,1} - (D_{2,1} + D_{2,5})D_{3,2}) \\ &-2D_{2,3}((D_{1,2} + D_{1,4})D_{3,1} - (D_{1,1} + D_{1,5})D_{3,2}) \\ &-D_{3,3}((D_{1,1} + D_{1,5})(D_{2,2} + D_{2,4}) - (D_{1,2} + D_{1,4})(D_{2,1} + D_{2,5})) = 0. \end{aligned} \tag{4.6b}$$

These two equations are once again decoupled from each other. The second equation yields the complex wavenumbers associated with the axisymmetric mode and the first and second helical modes. The first equation yields the complex wavenumbers associated with the first and second helical modes with opposite sign. In contrast to the previous three mode case, the axisymmetric mode is also affected by λ. Furthermore, not only do we see once again that the dispersion relations for positive and negative

first helical modes are different from one another, but we also find that the same is true for the second helical mode.

The analysis of the dispersion relation becomes too complex to allow simple analytical equations such as (4.6) when more modes are considered. Nevertheless, it turns out that the symmetry structure ($D^{(N)}_{i,j} = D^{(N)}_{N+1-i,N+1-j}$) of the dispersion relation matrix is maintained when more modes are included in the analysis ($m = \pm 3, \pm 4$, and so on). As a direct consequence, the dispersion relation can be split into two different equations for these cases, as in (4.6), and the dispersion relations for positive and negative helical modes again are different. Although this does not guarantee that the growth rates of positive and negative helical modes will be different for arbitrary values of x_0, St and λ, these observations are strong indications that this may well be the case.

Ultimately, symmetry of the transverse jet is still an open question in the literature. The results above show that the transverse jet is inherently asymmetric in the sense discussed at the beginning of this subsection, not even possessing a plane of symmetry as often assumed in simulations (e.g. Cortelezzi & Karagozian 2001). On the other hand, although the growth rates of the positive and negative helical modes are indeed different, an evaluation of equations (4.6) reveals that this difference is small for both first and second helical modes. Hence, the transverse jet may be only weakly asymmetric. This discovery may explain some seemingly contradictory features of the transverse jet. While the early experiments of Kamotani & Greber (1974) suggest that the CVP is a symmetric structure, for example, Kuzo (1995) and Smith & Mungal (1998) provide experimental evidence indicating that the CVP can be either symmetric or asymmetric. The concept of symmetry described in the current analysis, via the initiation and coupling of non-axisymmetric modes, may provide an explanation for the origin of the CVP's asymmetry.

5. Discussion and conclusions

In this paper the near field of the inviscid jet in crossflow is used as a baseflow for a local, linear stability analysis. The approach employs a Fourier transformation of the stability problem, which takes into account the coupling, due to the baseflow, between different azimuthal modes. The study provides a mathematical foundation for and evidence associated with transverse jet behaviour and shear layer instabilities that have heretofore not been well understood.

This multiple mode analysis indicates that the axisymmetric instability mode of the transverse jet upstream shear layer is destabilized by the crossflow, and that this effect is caused by the linear coupling between this axisymmetric mode and the helical modes. The destabilizing effect of the crossflow, even at very low crossflow-to-jet velocity ratios λ, suggests a fundamental difference between convective shear layer instabilities associated with the free jet and with the transverse jet. As noted above, such convective instabilities for the transverse jet are observed in experiments to occur closer to the jet orifice than those associated with the free jet, and as crossflow magnitude increases, the instability is strengthened in magnitude, even for relatively low values of λ, on the order of 0.1–0.15 (Megerian *et al.* 2006).

The off-diagonal terms introduced by the crossflow in the otherwise diagonal dispersion matrix in the present analysis allow us to use this matrix's diagonal dominance as a quantitative criterion to estimate the critical velocity ratio below which the free and transverse jet shear layers can still be considered mathematically similar. This criterion suggests that this critical value of crossflow-to-jet velocity ratio may be as small as $\lambda_c \simeq 0.0036$, indicating that the transverse jet shear layer and

vortex rollup and merger can be fundamentally different from those for the free jet even for extremely small crossflow velocities.

The present analysis also demonstrates that positive and negative helical modes for the transverse jet have slightly different growth rates, implying a lack of symmetry for the transverse jet Kelvin–Helmholtz instability and hence the evolving vortex rings. This might explain the lack of symmetry of the (mean) CVP observed under some conditions in the literature (Kuzo 1995; Smith & Mungal 1998), since most researchers consider the Kelvin–Helmholtz instability and associated evolution of vortex rings to play an important role in CVP formation. To our knowledge this is the first mathematical verification that even low-level crossflows can produce weak asymmetries in the transverse jet.

While the present results provide an interesting theoretical perspective on the differences between free jet and transverse jet shear layer instabilities, there are still important issues that require exploration. As noted from the beginning, the linear stability analysis of a flow field represented by a discontinuous (inviscid) baseflow as done in the present study is valid for low Strouhal numbers and does not predict the conditions for which maxima in the growth rates of various modes occur. The stability analysis of the transverse jet as represented with a continuous baseflow, which provides the potential for the exploration of maxima in the growth rates, as well as changes in the conditions producing the maxima depending on the transverse jet configuration, is described in Alves *et al.* (2006), while results from a full three-dimensional time-dependent numerical simulation of the transverse jet near field are available in Alves (2006).

The authors would like to acknowledge the financial support of CAPES/Brazil, the UCLA Graduate Division, the National Science Foundation under Grants CTS-0200999 and CTS-0457413 and NASA under Grant NCC-157.

Appendix. Dispersion relation matrix

In this Appendix, the elements of the multiple mode dispersion matrix (4.3) derived in § 4.2 for the three mode case are written out. However, these matrix elements are remarkably complex even when only three modes are considered. In order to simplify the presentation of these results while still allowing the reader to evaluate the different transverse jet dispersion relations, the terms of order λ^3 and higher present in these matrix elements are neglected. The matrix elements of the five mode case are not presented because they are too long and complex even when neglecting terms of order λ^3 or higher.

The elements of dispersion matrix (4.3) are

$$D_{1,1} = 2\pi \mathrm{i} \frac{\omega^2 \left(I_0(\alpha) + I_2(\alpha)\right) K_1(\alpha) + (\alpha - \omega)^2 \left(K_0(\alpha) + K_2(\alpha)\right) I_1(\alpha)}{\omega \left(I_0(\alpha) + I_2(\alpha)\right)}, \tag{A 1}$$

$$\begin{aligned} D_{1,3} = \pi\lambda^2 \big(&2\alpha\omega(I_0(\alpha) + I_2(\alpha))^2 \big((C_2 - x_0)\alpha^2 K_0(\alpha) + (2(C_2 - x_0) - \mathrm{i}\alpha)\omega K_1(\alpha) \\ &+ (C_2 - x_0)\alpha^2 K_2(\alpha)\big) + \mathrm{i}\alpha\omega(I_0(\alpha) + I_2(\alpha))^2 \big(\alpha^2(\alpha - 2\omega)K_0(\alpha) + 4\omega^2 K_1(\alpha) \\ &+ \alpha^2(\alpha - 2\omega)K_2(\alpha)\big) R_{j,2}(x_0) - \mathrm{i}(\alpha - \omega)^2 \omega I_1(\alpha)(I_0(\alpha) + I_2(\alpha))(-4\alpha K_0(\alpha) \\ &+ (3\alpha^2 - 8)K_1(\alpha) + \alpha(\alpha K_3(\alpha) - 4K_2(\alpha))R_{j,2}(x_0) + I_1(\alpha)(K_0(\alpha) + K_2(\alpha)) \\ (-2(2(C_2 - x_0) - \mathrm{i}\alpha)\alpha(\alpha^2 - 4\alpha\omega + 3\omega^2)&(I_0(\alpha) + I_2(\alpha)) - \mathrm{i}(3\alpha^2 - 8)(\alpha - \omega)^2 \\ &\omega I_1(\alpha) R_{j,2}(x_0) - \mathrm{i}\alpha^2(\alpha - \omega)^2 \omega I_3(\alpha) R_{j,2}(x_0))/(2\alpha\omega^2(I_0(\alpha) + I_2(\alpha))^2), \end{aligned} \tag{A 2}$$

$$D_{2,2} = 2\pi\mathrm{i}\frac{\omega^2 I_1(\alpha)K_0(\alpha) + (\alpha-\omega)^2 I_0(\alpha)K_1(\alpha)}{\omega I_1(\alpha)}, \tag{A 3}$$

$$D_{2,3} = \pi\lambda\frac{(\alpha-\omega)^2(K_0(\alpha)+K_2(\alpha))I_0(\alpha) - 2\omega^2 I_1(\alpha)K_1(\alpha)}{\omega^2 I_1(\alpha)}, \tag{A 4}$$

where $I_m(\alpha)$ and $K_m(\alpha)$ are modified Bessel functions.

REFERENCES

de B. Alves, L. S. 2006 Transverse jet shear-layer instabilities: Linear stability analysis and numerical simulations. PhD thesis, University of California at Los Angeles, Los Angeles, USA.

de B. Alves, L. S., Kelly, R. E. & Karagozian, A. R. 2006 Transverse jet shear-layer instabilities. Part 2. Linear analysis for large jet-to-crossflow velocity ratio. *J. Fluid Mech.* (submitted).

Batchelor, G. K. & Gill, A. E. 1962 Analysis of the stability of axisymmetric jets. *J. Fluid Mech.* **14**, 529–551.

Blanchard, J. N., Brunet, Y. & Merlen, A. 1999 Influence of a counter rotating vortex pair on the stability on a jet in cross flow: An experimental study by flow visualizations. *Exps. Fluids* **26**, 63–74.

Blossey, P. N. & Schmid, P. J. 2002 Global stability analysis of a jet in cross flow. *Bull. Am. Phys. Soc.* **47**(10), 92.

Chandrasekhar, S. 1961 *Hydrodynamic and Hydromagnetic Stability*. Oxford University Press.

Coelho, S. L. V. 1988 The dynamics of the near field of entraining jets in cross flows. PhD thesis, University of Cambridge.

Coelho, S. L. V. & Hunt, J. C. R. 1989 The dynamics of the near field of strong jets in cross flow. *J. Fluid Mech.* **200**, 95–120.

Corke, T. C. & Kusek, S. M. 1993 Resonance in axisymmetric jets with controlled helical-mode input. *J. Fluid Mech.* **249**, 307–336.

Corke, T. C., Shakib, F. & Nagib, H. M. 1991 Mode selection and resonant phase locking untable axisymmetric jets. *J. Fluid Mech.* **223**, 253–311.

Cortelezzi, L. & Karagozian, A. R. 2001 On the formation of the counter-rotating vortex pair in transverse jets. *J. Fluid Mech.* **446**, 347–373.

Crow, S. C. & Champagne, F. M. 1971 Orderly structure in jet turbulence. *J. Fluid Mech.* **48**, 547–591.

Drazin, P. G. & Reid, W. H. 1981 *Hydrodynamic Stability*. Cambridge University Press.

Fric, T. F. & Roshko, A 1994 Vortical structure in the wake of a transverse jet. *J. Fluid Mech.* **279**, 1–47.

Godrèche, C. & Manneville, P. 1998 *Hydrodynamics and Nonlinear Instabilities*. Cambridge University Press.

Huerre, P. & Monkewitz, P. A. 1990 Local and global instabilities in spatially developing flows. *Annu. Rev. Fluid Mech.* **22**, 473–537.

Huq, P. & Dhanak, M. R. 1996 The bifurcation of circular jets in cross flow. *Phys. Fluids* **8** (3), 754–763.

Kamotani, Y. & Greber, I. 1974 Experiments on confined turbulent jets in a cross flow. *Tech. Rep.* CR - 2392. NASA.

Karagozian, A. R., Cortelezzi, L. & Soldati, A. 2003 *Manipulation and Control of Transverse Jets*. CISM Courses and Lectures, vol. 439. Springer.

Kelso, R. M., Lim, T.T. & Perry, A. E. 1996 An experimental study of round jets in cross flow. *J. Fluid Mech.* **306**, 111–144.

Kuzo, D. M. 1995 An experimental study of the turbulent transverse jet. PhD thesis, California Institute of Technology.

Lin, S. P. 2003 *Breakup of Liquid Sheets and Jets*. Cambridge University Press.

Margason, R. J. 1993 Fifty years of jet in cross flow research. *AGARD-CP*-534 **1**, 1–141.

Megerian, S., Davitian, J., de B. Alves, L. S. & Karagozian, A. R. 2006 Transverse jet shear-layer instabilities. Part I) experimental studies. *J. Fluid Mech.* (submitted).

MICHALKE, A. 1971 Instabilität eines kompressiblen runden freistrahls unter berücksichtigung des einflusses der strahlgrenzschichtdicke. *Z. Flugwiss.* **19** (8–9), 319–328, English translation: NASA TM 75190 (1977).

NEEDHAM, D. J., RILEY, N. & SMITH, J. H. B. 1988 A jet in cross flow. *J. Fluid Mech.* **188**, 159–184.

SMITH, S. H. & MUNGAL, M. G. 1998 Mixing, structure and scaling of the jet in cross flow. *J. Fluid Mech.* **357**, 83–122.

WOLFRAM, S. 1999 *The Mathematica Book*, 4th edn. Cambridge: Wolfram Media.